A Journal of the Gesellschaft Deutscher Chemiker

Angewandte International Edition Chemie

GDCh

www.angewandte.org

Accepted Article

Title: Self-organized Ruthenium-Barium Core-Shell Nanoparticles on a Mesoporous Calcium Amide Matrix for Efficient Low-Temperature Ammonia Synthesis

Authors: Masaaki Kitano, Yasunori Inoue, Masato Sasase, Kazuhisa Kishida, Yasukazu Kobayashi, Kohei Nishiyama, Tomofumi Tada, Shigeki Kawamura, Toshiharu Yokoyama, Michikazu Hara, and Hideo Hosono

To be cited as: *Angew. Chem. Int. Ed.* 10.1002/anie.201712398
Angew. Chem. 10.1002/ange.201712398

Link to VoR: http://dx.doi.org/10.1002/anie.201712398
http://dx.doi.org/10.1002/ange.201712398

WILEY-VCH

10.1002/anie.201712398

WILEY-VCH

COMMUNICATION

Self-organized Ruthenium-Barium Core-Shell Nanoparticles on a Mesoporous Calcium Amide Matrix for Efficient Low-Temperature Ammonia Synthesis

Masaaki Kitano[+], Yasunori Inoue[+], Masato Sasase, Kazuhisa Kishida, Yasukazu Kobayashi, Kohei Nishiyama, Tomofumi Tada, Shigeki Kawamura, Toshiharu Yokoyama, Michikazu Hara*, and Hideo Hosono*

Dedication ((optional))

Abstract: A low-temperature ammonia synthesis process is required for on-site synthesis. Here, we report that barium-doped calcium amide (Ba-$Ca(NH_2)_2$) significantly enhances the ammonia synthesis activities of Ru and Co by two-orders of magnitude more than that of a conventional Ru catalyst below 300ºC. Furthermore, the present catalysts are superior to that of the wüstite-based Fe catalyst known as a highly active industrial catalyst at low temperatures and pressures. Nanosized Ru-Ba core-shell structures are self-organized on the support during hydrogen pretreatment, and the support material is simultaneously converted into a mesoporous structure with a high surface area (>100 m^2 g^{-1}). These unique self-organized nanostructures account for the high catalytic performance in low-temperature ammonia synthesis.

Nitrogen (N_2) activation to ammonia (NH_3) is a key technology for supporting human life because NH_3 is used as a source for the production of synthetic fertilizers, nitric acid, and nitrogen-containing chemicals.[1] Owing to strong N≡N bond, industrial NH_3 synthesis (Haber-Bosh process) must be conducted using promoted iron-based catalysts at high reaction temperatures (400-500ºC).[2] Furthermore, high pressure (10-30 MPa) is required due to thermodynamic limitations. As a result, large-scale and robust plants are required for the Haber-Bosh process. In the past few years, many researchers have focused on the development of an efficient process for NH_3 synthesis under milder reaction conditions. Low temperatures are thermodynamically favorable for high NH_3 production and small-scale NH_3 synthesis process has been in recent demand for on-site ammonia production. Low temperature NH_3 synthesis has been investigated using organometallic complexes, photocatalysts, plasma, and electrochemical methods.[3] Although some of these systems have succeeded in N_2 reduction to NH_3, even at room temperature, the efficiency and stability are still insufficient for industrial application. Ru-based catalysts are well known as efficient catalysts that function under milder reaction conditions than those used with the Fe-based catalyst process.[4] However, Ru-based catalysts exhibit much lower activity than Fe-based catalysts, especially at low reaction temperatures (<370ºC).[2a] Ru-based catalysts are strongly inhibited by hydrogen adsorption at low reaction temperatures;[5] therefore, there have been many recent attempts to overcome the drawbacks of Ru catalysts and realize low temperature NH_3 synthesis.[6]

We have recently reported that electrides, hydrides (Ca_2NH), and calcium amides ($Ca(NH_2)_2$) significantly promote the activity of Ru catalysts at low reaction temperatures with low activation energy (50–60 kJ mol^{-1}) when these materials are used as catalyst supports.[7] These materials typically have very low work functions (WFs; 2.3–3.5 eV), which provide electrons to Ru to enhance the N_2 dissociation. Furthermore, hydride ions (H^- ions) are formed in these catalysts and reversible reaction between H^- ions and anionic electrons occurs at the Ru-support interfaces during NH_3 synthesis.[7c] This smooth anion exchangeability suppresses hydrogen poisoning on the Ru surface. Another group also recently reported that composite catalysts containing transition metals (TM = Cr, Mn, Fe, Co) and hydride such as LiH and BaH_2 exhibit high catalytic activity and low activation energy (45–65 kJ mol^{-1}) for NH_3 synthesis, in which metal-N-H species (such as amides or imides) are formed as intermediates.[8] Thus, metal-N-H systems are considered as effective supports or promoter for NH_3 synthesis.[9] However, further effort is required to understand the origin of the high catalytic activity to develop a new way to enhance the catalytic performance.

Herein, we demonstrate that the activity of Ru-loaded $Ca(NH_2)_2$ for NH_3 synthesis can be significantly enhanced by the introduction of Ba into the $Ca(NH_2)_2$ matrix and H_2 treatment, which resulted in the highest activity ever reported for heterogeneous catalysts. Detailed characterization reveals that the Ru-Ba core-shell structure and the mesoporous structure of the support are self-organized during the H_2 pretreatment. Such a unique structural change is a key factor of the high catalytic performance.

Ba-doped $Ca(NH_2)_2$ was prepared by the reaction of Ca and Ba metal with liquid NH_3 at −40ºC, and the resultant solution was heated at 100ºC for 1 h. The obtained powder was then combined with Ru (to produce Ru/Ba-$Ca(NH_2)_2$) by heating with various Ru precursors under H_2 gas flow at 400ºC. As shown in Figure S1, the Ru/Ba-$Ca(NH_2)_2$ catalyst prepared using ruthenium(III) acetylacetonate ($Ru(acac)_3$) exhibits the highest activity for NH_3 synthesis. Figure S2 shows the effect of Ba-doping on the catalytic activity of Ru/Ba-$Ca(NH_2)_2$. A small amount of Ba-doping

[*] Prof. Dr. M. Kitano, Dr. M. Sasase, Dr. K. Kishida, Dr. Y. Kobayashi, K. Nishiyama, Prof. Dr. T. Tada, Dr. S. Kawamura, Dr. T. Yokoyama, Prof. Dr. H. Hosono
Materials Research Center for Element Strategy, Tokyo Institute of Technology, 4259 Nagatsuta, Midori-ku, Yokohama 226-8503, Japan
E-mail:hosono@msl.titech.ac.jp
[*] Dr. Y. Inoue, Prof. Dr. M. Hara, Prof. Dr. H. Hosono
Laboratory for Materials and Structures, Tokyo Institute of Technology, 4259 Nagatsuta, Midori-ku, Yokohama 226-8503, Japan
E-mail: hara.m.ae@m.titech.ac.jp
Dr. K. Kishida, Dr. Y. Kobayashi, Prof. Dr. M. Hara, Prof. Dr. H. Hosono
ACCEL, Japan Science and Technology Agency, 4-1-8 Honcho, Kawaguchi, Saitama, 332-0012, Japan
[+] These authors contributed equally to this work.

Supporting information for this article is given via a link at the end of the document.

10.1002/anie.201712398

COMMUNICATION

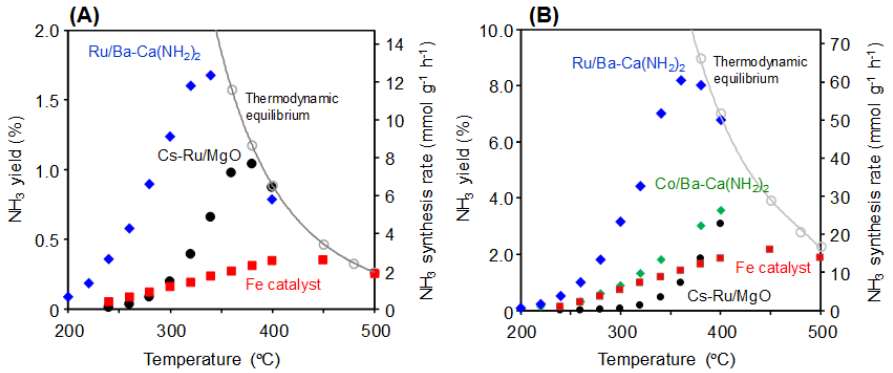

Figure 1. Temperature dependence of NH_3 synthesis activity of various catalysts at (A) 0.1 MPa and (B) 0.9 MPa. The amount of metal loading for Ru/Ba-Ca$(NH_2)_2$, Cs-Ru/MgO, and Co/Ba-Ca$(NH_2)_2$ were 10, 10, and 8 wt%, respectively.

(3 at%) was effective to enhance the activity of the Ru/Ca$(NH_2)_2$ catalyst, although Ru/Ba$(NH_2)_2$ has negligible activity.

Figure 1 shows the NH_3 synthesis activity of Ru(10 wt%)/Ba(3 at%)-Ca$(NH_2)_2$ as a function of reaction temperature at 0.1 and 0.9 MPa. The catalytic activity of Cs-Ru/MgO and an industrial benchmark Fe catalyst with the wüstite structure (Figure S3) are also shown in this figure. The wüstite-based catalyst is known to be more active than the magnetite-based catalyst at low-temperatures and low-pressures.[10] At atmospheric pressure (0.1 MPa), the activity of Cs-Ru/MgO, which is one of the most active Ru catalysts reported to date,[5b, 11] exceeded that of the Fe-based catalyst to a significant extent. However, this trend was reversed below 300ºC. On the other hand, Ru/Ba-Ca$(NH_2)_2$ exhibited much higher catalytic activity than the other catalysts, and the NH_3 concentration formed above 340ºC reached thermodynamic equilibrium. Furthermore, the catalytic activity of Ru/Ba-Ca$(NH_2)_2$ is much superior to those of other metal-amide based catalysts (Figure S4), indicating significant promoting effect of Ba-Ca$(NH_2)_2$.

The catalytic activities of Ru/Ba-Ca$(NH_2)_2$ were increased significantly at 0.9 MPa and the maximum NH_3 synthesis rate (60.4 mmol g^{-1} h^{-1}) was recorded at 360ºC, which is *ca.* 6 times higher than that of the Fe-based catalyst. Furthermore, Ru/Ba-Ca$(NH_2)_2$ works as an efficient catalyst for NH_3 synthesis below 300ºC, at which Cs-Ru/MgO exhibits negligibly low activity. For instance, the NH_3 synthesis rate (7.5 mmol g^{-1} h^{-1}) of Ru/Ba-Ca$(NH_2)_2$ at 260ºC is higher by two orders of magnitude than that of Cs-Ru/MgO (0.072 mmol g^{-1} h^{-1}). Ba-Ca$(NH_2)_2$ also effectively promotes the activity of the Co catalyst, which exceeds the catalytic performance of the Fe and Cs-Ru/MgO catalysts. It should be noted that Ru and Co-loaded Ba-Ca$(NH_2)_2$ catalysts exhibited significantly higher catalytic activity than state-of-the-art catalysts reported to date, not only with respect to NH_3 synthesis rate, but also the NH_3 yield (Table S1). These results demonstrate that the Ba-Ca$(NH_2)_2$ support functions as an efficient promoter of Ru and Co catalysts in low-temperature NH_3 synthesis. The activity of Cs-Ru/MgO was decreased slightly with an increase in the reaction pressure at low temperatures (200-340ºC) (Figure S5), which is attributed to hydrogen poisoning over the Ru catalyst. Conventional Ru catalysts are known to be sensitive to hydrogen adsorption in NH_3 synthesis, especially at low reaction temperatures, which results in the strong suppression of N_2 dissociation over the Ru catalyst.[5] The activity of Cs-Ru/MgO is consequently lower than that of the Fe-based catalyst at low reaction temperatures and elevated pressure (Figure 1B). In contrast, the activity of Ru/Ba-Ca$(NH_2)_2$ increased with the reaction pressure, even at 300ºC (Figure S6), indicating high resistance to hydrogen poisoning. Furthermore, the NH_3 synthesis rate of Ru/Ba-Ca$(NH_2)_2$ remained constant for 100 h (Figure S7), and the total amount of produced NH_3 reached 320 mmol (more than 260 times that with Ba-Ca$(NH_2)_2$), demonstrating the high durability of the catalyst. The activity of Ru/Ba-Ca$(NH_2)_2$ was decreased when it was exposed to air before reaction, whereas Ru/Ba-Ca$(NH_2)_2$ is relatively resistant to dry O_2 (Figure S8). Although new catalytic process needs to be developed, the present catalyst has a great impact on the study of ammonia synthesis.

The local structure of the Ru/Ba-Ca$(NH_2)_2$ catalyst after NH_3 synthesis was evaluated using high-angle annular dark-field scanning transmission electron microscopy (HAADF-STEM) and energy-dispersive X-ray spectroscopy (EDX). As shown in Figure 2A, small-sized Ru nanoparticles are highly dispersed and epitaxially attached onto the support material, which is analogous to our previous result for Ba-free Ru/Ca$(NH_2)_2$.[7d] The size of the Ru particles is mainly distributed in the range of 1.5–4.5 nm, which is much smaller than those of Ru/Ca$(NH_2)_2$ and Ru/Ba$(NH_2)_2$ (Figures S9 and S10). The catalytic properties of these materials are summarized in Table 1. The difference in the NH_3 synthesis rates of the tested catalysts is much larger than that of the Ru surface area; therefore, the high catalytic activity of Ru/Ba-Ca$(NH_2)_2$ cannot be explained only by the number of surface Ru sites. The turnover frequency (TOF) with Ru/Ba-Ca$(NH_2)_2$ is much superior to those of the other Ru catalysts, which suggests that the intrinsic activity of the Ru

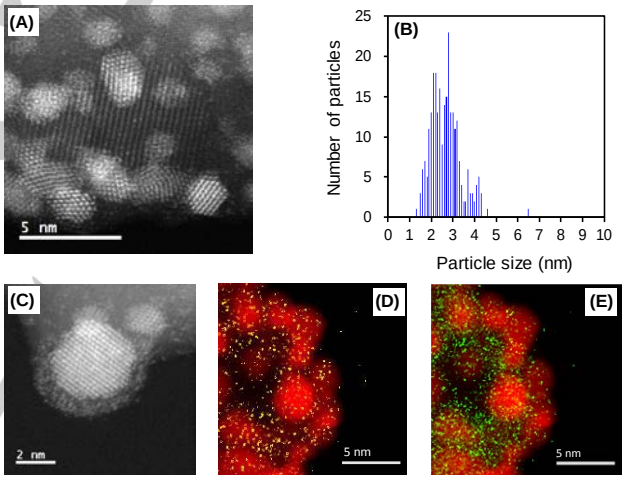

Figure 2. (A) HAADF-STEM image and (B) corresponding particle size distributions of Ru/Ba-Ca$(NH_2)_2$ after NH_3 synthesis. (C) Enlarged image of Ru particles on the catalyst surface. EDX elemental mapping images of (D) Ba (yellow) and (E) Ca (green), where Ru is displayed as red.

Table 1. Catalytic properties of various catalysts with 10 wt% Ru

Catalyst	*d* [nm][a]	A_m [m^2 g^{-1}][a]	r_{NH3} [mmol g^{-1} h^{-1}][b]	TOF [s^{-1}]
Ru/Ba-Ca$(NH_2)_2$	2.7	178.5	23.3	13.4 x 10^{-3}
	31.8	15.2		157.9 x 10^{-3}
Ru/Ca$(NH_2)_2$	4.4	109.5	5.7	5.3 x 10^{-3}
	14.2	33.9		17.1 x 10^{-3}
Ru/Ba$(NH_2)_2$	5.3	90.9	0.3	0.3 x 10^{-3}
	9.3	51.7		0.6 x 10^{-3}
Cs-Ru/MgO	5.2	92.7	0.4	0.4 x 10^{-3}
	9.8	49.0		0.8 x 10^{-3}

[a]Average Ru particle size (*d*) and the surface area of Ru per Ru weight (A_m) were determined by STEM measurements (upper) and H_2 chemisorption method (lower). [b]NH_3 synthesis rate (r_{NH3}); conditions: pressure (0.9 MPa), temperature (300ºC).

10.1002/anie.201712398

catalyst was significantly enhanced by the Ba-Ca$(NH_2)_2$ system. The surface area of Ru on each catalyst estimated by H_2 chemisorption is much smaller than that determined by STEM observation. This difference originates from the coverage of the Ru surface with the support material. Among the tested catalysts, Ru/Ba-Ca$(NH_2)_2$ has the lowest H_2 chemisorption sites although it has much smaller Ru particles observed in STEM image than the other catalysts. It should be noted that the Ru nanoparticles on Ba-Ca$(NH_2)_2$ are covered by a thin ca. 1 nm layer, which leads to the clear contrast between the core and shell (Figure 2C). This overlayer accounts for the low H_2 chemisorption, while it would possess porous structure to adsorb reactant gas molecules. EDX elemental mapping showed that both Ba and Ca species are distributed on the Ru particles (Figures 2D, E). The EDX line profile analysis also revealed that Ru is located at core region whereas the Ca and Ba signals are distributed throughout the entire particle (Figure S11). On the other hand, the core-shell structure was not observed for Ba-free Ru/Ca$(NH_2)_2$ and Ca-free Ru/Ba$(NH_2)_2$ (Figures S9 and S10). Accordingly, the lattice mismatch between Ca$(NH_2)_2$ and Ba$(NH_2)_2$ would contribute to the formation of the overlayer on the Ru nanoparticles.

The surface composition of the catalyst was examined using X-ray photoelectron spectroscopy (XPS). As summarized in Table S2, the Ba species is homogeneously distributed in the as-prepared Ba-Ca$(NH_2)_2$ (Ba/Ca = 0.03). In contrast, the Ba/Ca ratio of Ru/Ba-Ca$(NH_2)_2$ was much larger than 0.03, indicating that Ba species preferentially migrate to the catalyst surface via Ru, which leads to the formation of an overlayer on the Ru particles. X-ray diffraction (XRD) patterns for Ca$(NH_2)_2$, Ba$(NH_2)_2$, Ba-Ca$(NH_2)_2$, and Ru/Ca$(NH_2)_2$ after reaction (300ºC, 113 h), are shown in Figure S12. The XRD pattern of Ba-Ca$(NH_2)_2$ was almost identical to that of Ca$(NH_2)_2$, while weak peaks due to Ba$(NH_2)_2$ were also observed. The diffraction peaks significantly decreased, and Ca_2NH or CaNH phases were formed after the reaction, implying that the mixture of these crystal structures was formed after the reaction. In addition, broad peaks due to Ru were also observed, which indicates the formation of small-sized Ru particles.

Nitrogen adsorption-desorption isotherms and Barrett-Joyner-Halenda (BJH) pore size distributions of the catalyst are presented in Figure 3. The isotherms for Ba-Ca$(NH_2)_2$ before and after H_2 pretreatment at 400ºC are similar in shape to type II isotherms in IUPAC classification terms. The surface area of Ba-Ca$(NH_2)_2$ decreased after H_2 pretreatment (Table S2), which indicates sintering of the material during heat treatment. Notably, the isotherm for the Ru/Ba-Ca$(NH_2)_2$ catalyst has a distinct hysteresis loop at P/P_0 = 0.5-0.9 (type IV), which indicates that a high density of mesopores is formed in this material during H_2 pretreatment (Figure 3B). The surface areas of the Ru/Ba-Ca$(NH_2)_2$ catalysts increased steeply after H_2 treatment at 300ºC, as shown in Figure 3C. The drastic increase in the surface area is attributed to the formation of a mesoporous structure (Figure S13). As shown in Figure S14, Ru(acac)$_3$ was decomposed at 200–250ºC in a H_2 atmosphere. These results suggest that Ru nanoparticles are formed on the Ba-Ca$(NH_2)_2$ support above 250ºC during H_2 pretreatment, and a mesoporous structure is subsequently produced by partial decomposition of the Ba-Ca$(NH_2)_2$ support by the Ru catalyst. It should be noted that no such structural change was observed for Ru/Ba$(NH_2)_2$ (Figure S15, Table S2). Thus, we can conclude that the unique mesoporous structure is formed only by the reaction of Ru nanoparticles with Ca$(NH_2)_2$ during the H_2 pretreatment. Furthermore, the mesoporous structure remained unchanged during 113 h of reaction, demonstrating the excellent stability of the catalyst (Figure 3D).

Kinetic analyses were conducted to elucidate the reaction mechanism for NH_3 synthesis over Ru/Ba-Ca$(NH_2)_2$. Table S3 shows that the apparent activation energy for NH_3 synthesis over Ru/Ba-Ca$(NH_2)_2$ (59.4 kJ mol^{-1}) is almost one-half that of Cs-Ru/MgO (124.3 kJ mol^{-1}), which provides evidence that N_2 cleavage over Ru is effectively promoted by Ba-Ca$(NH_2)_2$. This value is close to those for Ru-loaded electrides (50-60 kJ mol^{-1})[7a, 7c] which implies a similar reaction mechanism, in which the formation of N-H_x species is the rate-limiting step.[7b] The rate-determining step (RDS) for NH_3 synthesis over the Ru/Ba-Ca$(NH_2)_2$ catalyst was studied based on the Langmuir-Hinshelwood mechanism.[12] As shown in Figures 4 and S16, the experimental data is well-fitted with the modeled rates, based on the assumption that the N-H_x (x = 1–3) formation reaction is the RDS. These results demonstrate that the RDS for NH_3 synthesis

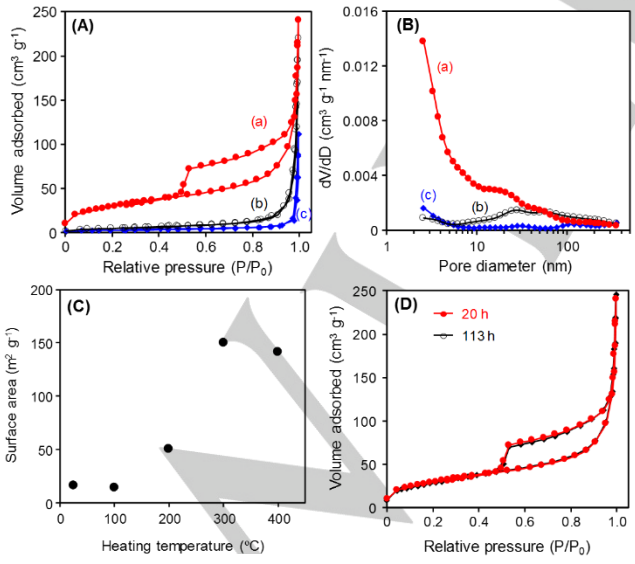

Figure 3. (A) Nitrogen adsorption-desorption isotherms and (B) BJH pore size distribution curves for (a) Ru/Ba-Ca$(NH_2)_2$, (b) Ba-Ca$(NH_2)_2$, and (c) Ba-Ca$(NH_2)_2$ after heat treatment at 400ºC and 0.1 MPa for 3h under H_2 gas flow. (C) Surface area of Ru/Ba-Ca$(NH_2)_2$ after heat treatment at various temperatures under H_2 gas flow. (D) Nitrogen adsorption-desorption isotherms for (a) Ru/Ba-Ca$(NH_2)_2$ after NH_3 synthesis at 300ºC for 20 h and 113 h.

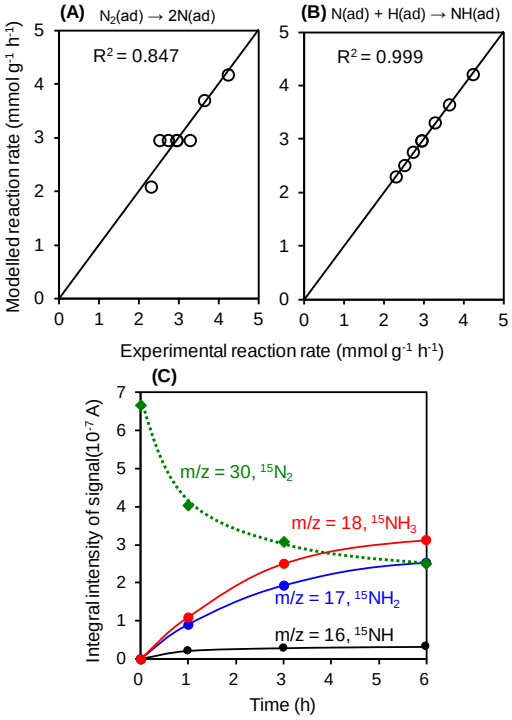

Figure 4. Best fit results for reaction rates over Ru/Ba-Ca$(NH_2)_2$ at 260ºC and 0.1 MPa with respect to the rate equations derived with different RDS (A: N_2 activation, B: NH formation). (C) Reaction time profiles for NH_3 synthesis from $^{15}N_2$ and H_2 over Ru/Ba-Ca$(NH_2)_2$ at 340ºC.

over Ru/Ba-Ca$(NH_2)_2$ could be any formation steps of N-H_x species rather than the N_2 dissociation step.[13]

The reaction orders with respect to N_2, H_2, and NH_3 are also listed in Table S3. Both the N_2 and H_2 reaction orders for Ru/Ba-Ca$(NH_2)_2$ are close to unity, and the reaction order of NH_3 is -0.92. This observation suggests that N-H_x species populate the catalyst surface more densely than N and H adatoms. This tendency is completely distinct from that for a conventional Ru catalyst such as Cs-Ru/MgO. The NH_3 order (-0.35) was less negative than the H_2 order (-0.50), which indicates that the surface of Cs-Ru/MgO is poisoned by hydrogen. Most Ru catalysts have a negative reaction order with respect to H_2 at low temperatures, whereas Ru/Ba-Ca$(NH_2)_2$ has a positive H_2 order, even at 260ºC. The unusual reaction order for Ru/Ba-Ca$(NH_2)_2$ is attributed to the unique core-shell structure shown in Figure 2C. Reversible exchange between hydride ions and electrons occur at Ru-Ca$(NH_2)_2$ interfaces, which imparts high tolerance to hydrogen poisoning.[7d] A similar reaction is considered to occur between Ru and Ba-Ca$(NH_2)_2$ shell. Next, the possibility of NH_3 formation from the Ba-Ca$(NH_2)_2$ support was investigated using isotopic $^{15}N_2$ and H_2. As $^{15}N_2$ decreased, the signals measured for m/z =18 and 17 increased with the intensity ratio in the range of 0.77-0.82 (Figure 4), where these signals were derived from $^{15}NH_3$. On the other hand, $^{14}NH_3$ was not produced by the reaction, which confirms that N atoms in Ba-Ca$(NH_2)_2$ are not used for NH_3 formation, but gas-phase N_2 molecules are activated over the Ru catalyst by electron donation from the Ba-Ca$(NH_2)_2$ support.

Density functional theory (DFT) calculations were performed to investigate the electron-donation ability of Ba-Ca$(NH_2)_2$. Table S4 summarizes the WFs and formation energies of NH_2 defects (E_{NH2def}) on Ca$(NH_2)_2$ (101) and Ba$(NH_2)_2$ (101) surfaces. The calculated WF for Ba$(NH_2)_2$ is smaller than that for Ca$(NH_2)_2$, which indicates the superior electron donating ability of Ba$(NH_2)_2$ over Ca$(NH_2)_2$. When an NH_2 unit was removed from the surface of each amide, the WFs of Ca$(NH_2)_2$ and Ba$(NH_2)_2$ were significantly reduced to 2.1 and 1.9 eV, respectively. Such a low WF is attributed to the formation of anionic electrons confined at the sites of NH_2 vacancies. Similar results were observed for other surfaces (Table S5). The calculated E_{NH2def} for Ba$(NH_2)_2$ is much smaller than that for Ca$(NH_2)_2$, which suggests that the formation of anionic electrons by NH_2 desorption as ammonia is much easier for Ba$(NH_2)_2$ than for Ca$(NH_2)_2$. Thus, by combining DFT calculations and STEM observations, low WF Ba$(NH_2)_{2-x}$ is formed near the Ru surface during H_2 pretreatment, which facilitates NH_3 synthesis over Ru/Ba-Ca$(NH_2)_2$ via electron donation from Ba$(NH_2)_{2-x}$ to Ru nanoparticles. Although the WF of anionic electrons at the Ba$(NH_2)_2$ surface is lower than that at Ca$(NH_2)_2$, the catalytic activity of the former is much lower than that of the latter (Table 1). No mesopore formation or epitaxial growth of Ru nanoparticles occurred for pure Ba$(NH_2)_2$, which could be due to the large lattice mismatch between Ru and Ba$(NH_2)_2$.

The improvement of the catalytic activity and stability of Ru/Ca$(NH_2)_2$ by Ba-doping has been already reported in our previous work,[7d] in which Ru/Ba-Ca$(NH_2)_2$ prepared by using $Ru_3(CO)_{12}$ was pretreated at 340ºC. The catalytic activity was not largely improved although the catalyst stability was significantly improved. The XPS analyses revealed that the surface Ba/Ca ratio of the Ru/Ba-Ca$(NH_2)_2$ in the current work is much higher than that of the previous catalyst (Table S2). The surface Ba species mainly contribute to the overlayer formation on the Ru nanoparticles (Figure 2), suggesting that the catalytic activity of surface Ru sites on the current Ru/Ba-Ca$(NH_2)_2$ are effectively enhanced by the surface Ba species rather than the case of the previous one. In addition, the present Ru/Ba-Ca$(NH_2)_2$ has a larger surface area (100 m^2 g^{-1}) than the previous catalyst (58 m^2 g^{-1}). The formation of Ru-Ba core-shell structure and the mesoporous structure with a large surface area can be caused by the H_2 pretreatment of Ba-Ca$(NH_2)_2$ with Ru(acac)$_3$ at 400ºC (Figure S17).

In summary, we have developed highly active and stable catalysts containing a Ba-Ca$(NH_2)_2$ support and Ru or Co nanoparticles for low-temperature NH_3 synthesis. The catalytic activity of Ru/Ba-Ca$(NH_2)_2$ is ca. 6 and 100 times higher than that of the industrial benchmark Fe catalyst (at 340ºC) and Cs-Ru/MgO (at 260ºC), respectively. Hydrogen pretreatment of the Ru/Ba-Ca$(NH_2)_2$ catalyst provides a mesoporous support structure and induces the formation of Ru-Ba core-shell structures. This unique structure is self-organized and stable for a long time. The overlayers derived from the Ba-Ca$(NH_2)_2$ support suppress H_2 poisoning at the Ru surface at low reaction temperatures *via* reversible exchange reaction between hydride ions and electrons. In addition, the formation of low-WF Ba$(NH_2)_{2-x}$ at the catalyst surface promotes N_2 dissociation over the Ru catalyst, which shifts the bottleneck in NH_3 synthesis from N_2 dissociation to N-H_x bond formation. The present results demonstrate that alkaline-earth amide materials can realize the optimal potential of transition metal catalysts for low-temperature NH_3 synthesis.

Acknowledgements

This work was supported by a fund from the Accelerated Innovation Research Initiative Turning Top Science and Ideas into High-Impact Values (ACCEL) program of the Japan Science and Technology Agency (JST), and the ENEOS Hydrogen Trust Fund. We appreciate the technical assistance of M. Okunaka and S. Fujimoto.

Keywords: Low-temperature ammonia synthesis • core-shell structure • mesoporous • alkaline earth metal amide • ruthenium

[1] J. M. Thomas, W. J. Thomas, *Principles and practice of heterogeneous catalysis*, John Wiley & Sons, **2014**.

[2] a) H. Liu, *Ammonia synthesis catalysts: innovation and practice*, World Scientific, **2013**; b) T. Kandemir, M. E. Schuster, A. Senyshyn, M. Behrens, R. Schlögl, *Angew. Chem. Int. Ed.* **2013**, *52*, 12723-12726.

[3] a) D. V. Yandulov, R. R. Schrock, *Science* **2003**, *301*, 76-78; b) K. Arashiba, Y. Miyake, Y. Nishibayashi, *Nat. Chem.* **2011**, *3*, 120-125; c) K. T. Ranjit, T. K. Varadarajan, B. Viswanathan, *J. Photochem. Photobiol., A* **1996**, *96*, 181-185; d) G. L. Wendt, J. E. Snyder, *J. Am. Chem. Soc.* **1928**, *50*, 1288-1292; e) C. J. M. van der Ham, M. T. M. Koper, D. G. H. Hetterscheid, *Chem. Soc. Rev.* **2014**, *43*, 5183-5191.

[4] a) K. Aika, A. Ozaki, H. Hori, *J. Catal.* **1972**, *27*, 424-431; b) A. Ozaki, *Acc. Chem. Res.* **1981**, *14*, 16-21; c) K. Aika, *Catal. Today* **2017**, *286*, 14-20; d) G. Prieto, F. Schüth, *Angew. Chem. Int. Ed.* **2015**, *54*, 3222-3239; e) N. Saadatjou, A. Jafari, S. Sahebdelfar, *Chem. Eng. Commun.* **2015**, *202*, 420-448.

[5] a) S. E. Siporin, R. J. Davis, *J. Catal.* **2004**, *225*, 359-368; b) F. Rosowski, A. Hornung, O. Hinrichsen, D. Herein, M. Muhler, G. Ertl, *Appl. Catal., A* **1997**, *151*, 443-460.

[6] a) K. Sato, K. Imamura, Y. Kawano, S. Miyahara, T. Yamamoto, S. Matsumura, K. Nagaoka, *Chem. Sci.* **2017**, *8*, 674-679; b) R. Manabe, H. Nakatsubo, A. Gondo, K. Murakami, S. Ogo, H. Tsuneki, M. Ikeda, A. Ishikawa, H. Nakai, Y. Sekine, *Chem. Sci.* **2017**, *8*, 5434-5439.

[7] a) M. Kitano, Y. Inoue, Y. Yamazaki, F. Hayashi, S. Kanbara, S. Matsuishi, T. Yokoyama, S. W. Kim, M. Hara, H. Hosono, *Nat. Chem.* **2012**, *4*, 934-940; b) M. Kitano, S. Kanbara, Y. Inoue, N. Kuganathan, P. V. Sushko, T. Yokoyama, M. Hara, H. Hosono, *Nat. Commun.* **2015**, *6*, 6731; c) M. Kitano, Y. Inoue, H. Ishikawa, K. Yamagata, T. Nakao, T. Tada, S. Matsuishi, T. Yokoyama, M. Hara, H. Hosono, *Chem. Sci.* **2016**, *7*, 4036-4043; d) Y. Inoue, M. Kitano, K. Kishida, H. Abe, Y. Niwa, M. Sasase, Y. Fujita, H. Ishikawa, T. Yokoyama, M. Hara, H. Hosono, *ACS Catal.* **2016**, *6*, 7577-7584.

[8] a) P. K. Wang, F. Chang, W. B. Gao, J. P. Guo, G. T. Wu, T. He, P. Chen, *Nat. Chem.* **2017**, *9*, 64-70; b) W. B. Gao, P. K. Wang, J. P. Guo, F.

10.1002/anie.201712398

Chang, T. He, Q. R. Wang, G. T. Wu, P. Chen, *ACS Catal.* **2017**, *7*, 3654-3661.

[9] a) P. L. Bramwell, S. Lentink, P. Ngene, P. E. de Jongh, *J. Phys. Chem. C* **2016**, *120*, 27212-27220; b) R. Michalsky, A. M. Avram, B. A. Peterson, P. H. Pfromm, A. A. Peterson, *Chem. Sci.* **2015**, *6*, 3965-3974; c) K. Aika, A. Ozaki, *J. Catal.* **1974**, *35*, 61-65.

[10] H. Z. Liu, X. N. Li, Z. N. Hu, *Appl. Catal., A* **1996**, *142*, 209-222.

[11] a) K. Aika, A. Ohya, A. Ozaki, Y. Inoue, I. Yasumori, *J. Catal.* **1985**, *92*, 305-311; b) K. Aika, T. Takano, S. Murata, *J. Catal.* **1992**, *136*, 126-140.

[12] I. Langmuir, *T. Faraday. Soc.* **1922**, *17*, 0621-0654.

[13] Y. Kobayashi, M. Kitano, S. Kawamura, T. Yokoyama, H. Hosono, *Catal. Sci. Technol.* **2017**, *7*, 47-50.

10.1002/anie.201712398

WILEY-VCH

COMMUNICATION

Entry for the Table of Contents (Please choose one layout)

Layout 1:

Ru-Ba core-shell nanoparticles and a mesoporous calcium amide matrix are self-organized during H_2 treatment of Ru/Ba-Ca$(NH_2)_2$, which imparts much higher catalytic performance for low-temperature ammonia synthesis than other Ru catalysts and an industrial Fe catalyst.

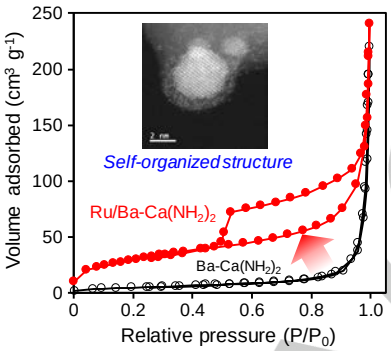

*Masaaki Kitano, Yasunori Inoue, Masato Sasase, Kazuhisa Kishida, Yasukazu Kobayashi, Kohei Nishiyama, Tomofumi Tada, Shigeki Kawamura, Toshiharu Yokoyama, Michikazu Hara, and Hideo Hosono**

Page 1. – Page 5.

Self-organized Ruthenium-Barium Core-Shell Nanoparticles on a Mesoporous Calcium Amide Matrix for Efficient Low-Temperature Ammonia Synthesis